Infrared spectrum of an extremely cool white-dwarf star

S. T. Hodgkin*†, B. R. Oppenheimer‡, N. C. Hambly§, R. F. Jameson*, S. J. Smartt‖† & I. A. Steele¶

** Department of Physics and Astronomy, University of Leicester, University Road, Leicester LE1 7RH, UK*
‡ Department of Astronomy, University of California-Berkeley, 601 Campbell Hall, Berkeley, California 94720, USA
§ Institute for Astronomy, University of Edinburgh, Blackford Hill, Edinburgh EH9 3HJ, UK
‖ Isaac Newton Group of Telescopes, Apartado de Correos 321, 38770 Santa Cruz de La Palma, La Palma, Islas Canarias, Spain
¶ Astrophysics Research Institute, Liverpool John Moores University, Twelve Quays House, Egerton Wharf, Birkenhead L41 1LD, UK
† Institute of Astronomy, Cambridge University, Madingley Road, Cambridge CB3 0HA, UK

White dwarfs are the remnant cores of stars that initially had masses of less than 8 solar masses. They cool gradually over billions of years, and have been suggested[1,2] to make up much of the 'dark matter' in the halo of the Milky Way. But extremely cool white dwarfs have proved difficult to detect, owing to both their faintness and their anticipated similarity in colour to other classes of dwarf stars. Recent improved models[3–5] indicate that white dwarfs are much more blue than previously supposed, suggesting that the earlier searches may have been looking for the wrong kinds of objects. Here we report an infrared spectrum of an extremely cool white dwarf that is consistent with the new models. We determine the star's temperature to be 3,500 ± 200 K, making it the coolest known white dwarf. The kinematics of this star indicate that it is in the halo of the Milky Way, and the density of such objects implied by the serendipitous discovery of this star is consistent with white dwarfs dominating the dark matter in the halo.

While white dwarfs may be the predominant component of the dark matter, they can also constrain the age of the Galaxy. The temperature below which the oldest white dwarfs have not yet had time to cool leads to a cut-off in the luminosity function of these objects. This cut-off has been observed[6] using white dwarfs drawn from the Luyten Half-Second Catalogue[7]. The turnover at visual magnitude $M_V = 16$, or effective temperature $T_e \approx 4{,}000$ K, implies an age of 6.5–11 Gyr for the Galactic disk[8–10]. However, if this sample is incomplete, then these ages are underestimates[11]. Indeed, more recent surveys[12–14] indicate a density of cool white dwarfs (with temperatures of about 4,000 K) that is higher by a factor of ~5. Early studies of the first luminosity function[6] and the Hubble Deep Field survey[15–17] showed little evidence for a substantial population of extremely cool (that is, Galactic halo) white dwarfs[9,18,19]. The new models[3–5] show that these surveys, which looked for red objects, excluded cool white dwarfs.

Two independent models of white-dwarf atmospheres[3–5] stress the dramatic effect of collision-induced absorption by molecular hydrogen on the spectra of very cool, hydrogen-rich white dwarfs. At effective temperatures below 4,000 K, H_2 molecules become abundant in the atmosphere, and, as the collision-induced absorption bands deepen, the peak of the resultant energy distribution shifts to the blue.

A low-luminosity, cool, white dwarf in Taurus, WD0346+246, was serendipitously discovered[20] from its large proper motion (1.27 ± 0.04 arcsec yr^{-1}) revealed in UK Schmidt Telescope photographic plates. Initial optical photometry and spectroscopy suggested a temperature ⩽4,000 K. We have subsequently obtained infrared photometry and spectra (Fig. 1) and the parallax is now known: 36 ± 5 mas, or a distance of $d = 28 \pm 4$ pc (ref. 21).

The spectral energy distribution presented in Fig. 1 certainly fulfills the expectations of the new theories[3–5], though no model spectra at this low a T_e have yet been reported to enable detailed comparison. (We note that another white dwarf, LHS3250, has recently been observed which shows strong H_2 collision-induced absorption opacity[22].)

In the absence of a suitable theoretical model, we can use simple arguments to determine T_e, the luminosity, L, and the radius, r, of the white dwarf, before estimating its mass and age. We fit the optical (wavelengths 0.4–0.8 μm) spectrum with a black body, and derive a temperature of 3,850 ± 100 K. This temperature is solely a parameter used to constrain the actual T_e, the mean radiative

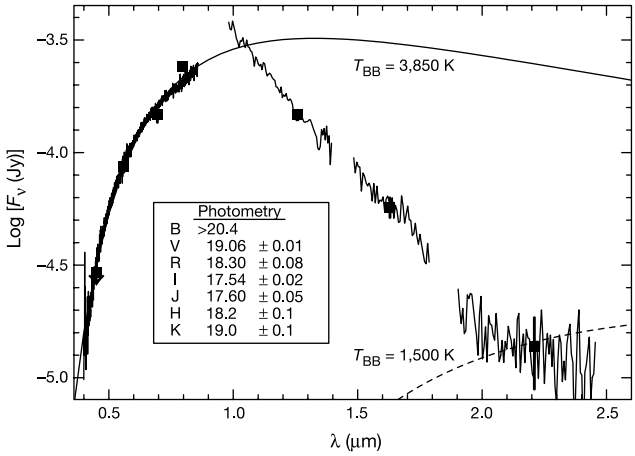

Figure 1 Spectrum of the cool white dwarf WD0346+246. Symbols with error bars are the photometric data from the Jacobus Kapteyn Telescope (JKT) (optical)[20] and the UK Infrared Telescope (UKIRT) (infrared), obtained in November 1998. The B-band is an upper limit. The optical spectrum is from ref. 20. We obtained the infrared spectrum with the NIRC[30] instrument at the W. M. Keck I Observatory (Hawaii) in February 1999. It covers 1–2.5 μm at a resolution of $\lambda/\Delta\lambda \approx 150$. The Keck photometric measurements (not shown) agree with the UKIRT values given here. Two fits to the data obtained with a blackbody model are overlaid at $T_{BB} = 3{,}850$ K (solid curve) and $T_{BB} = 1{,}500$ K (dashed curve). This large difference in brightness temperature over the wavelength range plotted demonstrates the effects of H_2 collision-induced absorption in the infrared. We have no explanation for the apparent excess of flux above the blackbody value at around 1 μm, but we note that models of H_2–He collision-induced absorption[23] show a reduction in opacity at wavelengths just short of 1 μm for atmospheres cooler than 4,000 K, and that synthetic spectra[5] show an excess even for white dwarfs with effective temperatures of about 4,000 K. However, uncertainties in the calibration of the spectra may play a role.

temperature, defined by $L = 4\pi r^2 \sigma T_e^4$, where σ is the Stefan–Boltzmann constant. This blackbody fit is expected in the optical, as H^- is the dominant opacity source here and because it has a very weak wavelength dependence. We can then write:

$$f_{0.4-0.8} = \frac{r^2}{d^2} F_{0.4-0.8}(T = 3{,}850\,\mathrm{K}) \quad (1)$$

where f is the observed flux, F the blackbody flux and d the distance. Our fitting technique constrains r/d to a precision of about 10%. For a white-dwarf atmosphere with a temperature of <4,000 K, the H_2 collision-induced absorption opacity increases by almost two orders of magnitude over the wavelength range 1–2 μm; at greater wavelengths it flattens[23]. So we once again expect a blackbody spectrum at wavelengths above 2 μm. Knowing r/d and the 2.2-μm flux, we find the temperature of this black body to be 1,500 K. This can be used to determine the contribution to the bolometric flux by the long-wavelength spectrum up to 5 μm. Beyond 5 μm, collision-induced absorption opacity becomes less important, and the spectrum will once again be dominated by the hotter and deeper regions of the star's atmosphere. We find the bolometric flux, f_{bol}, by integrating the flux from 0.4 to 2.5 μm and adding blackbody components for the regions outside our spectral coverage (we use a linear interpolation over the gap in the spectrum from 0.8 to 1 μm). These components are a 1,500 K black body from 2.5 to 5 μm, and a 3,850 K black body at wavelengths below 0.4 μm and beyond 5 μm. T_e is derived from f_{bol} by the following:

$$\sigma T_e^4 = f_{bol} \frac{d^2}{r^2} \quad (2)$$

This gives $T_e = 3{,}500 \pm 200$ K (minimum formal error). The contributions from the spectral region outside our coverage account for less than 8% of the total flux. Instead of using black bodies to account for this region, we could have linearly extrapolated the data beyond 2.5 μm. Furthermore, we might reasonably have discounted the excess flux around 1 μm (and attributed it to a calibration error). Both of these effects will make only small differences to our estimate of the temperature. Using the distance to WD0346+246 given in ref. 21, we find $L = 7.6(\pm 2.3) \times 10^{28}$ erg s^{-1}, or $L = 2.0(\pm 0.6) \times 10^{-5} L_\odot$, and $r = 0.012 \pm 0.002 R_\odot$ (here $L_\odot$ and $R_\odot$ are the solar luminosity and radius, respectively). The models[24] indicate a mass of $0.65 \pm 0.15 M_\odot$. Therefore WD0346+246 does not have a high mass (like ESO439–26[25]) and is probably a 'normal', albeit unusually cool, white dwarf. The location of WD0346+246 on the white-dwarf sequence in the M_V, $V–I$ diagram also supports this argument[21]. Estimating the age of WD0346+246 is difficult, as we lack important information concerning the atmosphere and core composition. However, the latest cooling models[4] suggest an age of about 12 Gyr, but with significant uncertainty.

The tangential velocity, v_t, of WD0346+246 provides evidence that it is a member of the Galactic halo. We have not measured a radial velocity for the object, nor are we able to because the spectrum lacks sharp features (such as those from atomic transitions). However, the arguments which follow are insensitive to assumptions about the radial velocity. The proper motion translates to a heliocentric tangential velocity $v_t \approx 170$ km s^{-1}. Allowing for the motion of the Sun with respect to the dynamical local standard of rest, v_t can be resolved into a velocity of ~60 km s^{-1} perpendicular to the Galactic plane (W), and ~150 km s^{-1} in the Galactic plane directed towards a Galactic longitude, $l = 270°$ (V). Local population I stars in the Galactic disk tend to orbit with velocities similar to the Sun's. The extremely large (V, W) velocity components of WD0346+246 are typical for a population II halo star[26].

Is this star simply a white dwarf associated with the known stars in the Galactic halo, or could it be part of a much greater number of white dwarfs accounting for a large fraction—or all—of the halo dark matter suggested by microlensing[2]? The known halo stars have a mass density of $5.6 \times 10^{-5} M_\odot$ pc^{-3} in the solar neighbourhood[27]. Assuming an initial mass function of slope –2.35 above 1 $M_\odot$ and –1.0 below 1 $M_\odot$ (ref. 28), the above mass density implies a number density of white dwarfs of 7×10^{-5} pc^{-3}, assuming that all stars more massive than 0.8 $M_\odot$ have become white dwarfs. If white dwarfs accounted for half of the measured halo dark matter, then the implied number density would need to be two orders of magnitude higher at 7.9×10^{-3} pc^{-3} (refs 2, 29). WD0346+246 is half a magnitude brighter than the I-plate limit[20], so similar objects could have been detected out to a distance of 35 pc, or a volume of ~100 pc^3 for one 5° × 5° photographic plate from the Schmidt telescope. Thus on one Schmidt plate we expect to see either 0.008 white dwarfs associated with the known Galactic halo stars, or 0.9 'dark matter' white dwarfs. This one serendipitous discovery on one plate clearly favours the latter possibility, but further survey work is needed for a definite conclusion. □

Received 7 June; accepted 15 November 1999.

1. Chabrier, G., Segretain, L. & Mera, D. Contribution of brown dwarfs and white dwarfs to recent microlensing observations and the halo mass budget. *Astrophys. J.* **468,** L21–L24 (1996).
2. Alcock, C. *et al.* The MACHO project Large Magellanic Cloud microlensing results from the first two years and the nature of the Galactic dark halo. *Astrophys. J.* **486,** 697–726 (1997).
3. Hansen, B. M. S. Old and blue white-dwarf stars as a detectable source of microlensing events. *Nature* **394,** 860–862 (1998).
4. Hansen, B. M. S. Cooling models for old white dwarfs. *Astrophys. J.* **502,** 680–695 (1999).
5. Saumon, D. & Jacobsen, S. B. Pure hydrogen model atmospheres for very cool white dwarfs. *Astrophys. J.* **511,** L107–L110 (1999).
6. Liebert, J., Dahn, C. C. & Monet, D. G. The luminosity fraction of white dwarfs. *Astrophys. J.* **332,** 891–909 (1988).
7. Luyten, W. J. *NLTT Catalog* (Univ. Minnesota Press, Minneapolis, 1979).
8. Winget, D. E. *et al.* An independent method for determining the age of the universe. *Astrophys. J.* **315,** L77–L81 (1987).
9. Wood, M. A. Constraints on the age and evolution of the Galaxy from the white dwarf luminosity function. *Astrophys. J.* **386,** 539–561 (1992).
10. Leggett, S. K., Ruiz, M. T. & Bergeron, P. The cool white dwarf luminosity function and the age of the Galactic Disk. *Astrophys. J.* **497,** 294–302 (1998).
11. Oswalt, T. D., Smith, J. A., Wood, M. A. & Hintzen, P. A lower limit of 9.5 Gyr on the age of the Galactic disk from the oldest white dwarf stars. *Nature* **382,** 692–694 (1996).
12. Knox, R. A., Hawkins, M. R. S. & Hambly, N. C. A survey for cool white dwarfs and the age of the Galactic Disk. *Mon. Not. R. Astron. Soc.* **306,** 636–752 (1999).
13. Ruiz, M. T. New cool degenerate stars. *Astron. J.* **111,** 1267–1270 (1996).
14. Festin, L. The luminosity function of white dwarfs and M dwarfs using dark nebulae as opaque outer screens. *Astron. Astrophys.* **336,** 883–894 (1998).
15. Flynn, C., Gould, A. & Bahcall, J. N. Hubble Deep Field constraint on baryonic dark matter. *Astrophys. J.* **466,** L55–L58 (1996).
16. Elson, R. A. W., Santiago, B. X. & Gilmore, G. F. Halo stars, starbursts, and distant globular clusters: A survey of unresolved objects in the Hubble Deep Field. *New Astron.* **1,** 1–16 (1996).
17. Mendez, R. A., Minniti, D., de Marchi, G., Baker, A. & Couch, W. J. Starcounts in the Hubble Deep Field: Constraining Galactic structure models. *Mon. Not. R. Astron. Soc.* **283,** 666–672 (1996).
18. Graff, D. S., Laughlin, G. & Freese, K. MACHOs, white dwarfs and the age of the universe. *Astrophys. J.* **499,** 7–19 (1998).
19. Tamanaha, C. M., Silk, J., Wood, M. A. & Winget, D. E. The white dwarf luminosity function—A possible probe of the Galactic Halo. *Astrophys. J.* **358,** 164–169 (1990).
20. Hambly, N. C., Smartt, S. J. & Hodgkin, S. T. WD0346+246: A very low luminosity, cool degenerate in Taurus. *Astrophys. J.* **489,** L157–L160 (1997).
21. Hambly, N. C. *et al.* On the parallax of WD0346+246: a Halo white dwarf candidate. *Mon. Not. R. Astron. Soc.* **309,** L33–L36 (1999).
22. Harris, H. C. *et al.* A very low-luminosity, very cool, DC white dwarf. *Astrophys. J.* **524,** 1000–1007 (1999).
23. Borysow, A., Jørgensen, U. G. & Zheng, C. Model atmospheres of cool, low-metallicity stars: the importance of collision-induced absorption. *Astron. Astrophys.* **324,** 185–195 (1997).
24. Wood, M. A. in *White Dwarfs* (eds Koester, D. & Werner, K.) 41–45 (Springer, Berlin Heidelberg, 1995).
25. Ruiz, M. T., Bergeron, P., Leggett, S. K. & Anguita, C. The extremely low luminosity white dwarf ESO 439-26. *Astrophys. J.* **455,** L159–L162 (1995).
26. Ryan, S. G. & Norris, J. E. Subdwarf studies. II—abundances and kinematics from medium resolution spectra. *Astron. J.* **101,** 1835–1864 (1991).
27. Dahn, C. C., Liebert, J., Harris, H. C. & Guetter, H. H. in *The Bottom of the Main Sequence—and Beyond* (ed. Tinney, C. G.) 239–248 (Springer, Berlin Heidelberg, 1995).
28. Gizis, J. E. & Reid, I. N. M subdwarfs: the population II luminosity function. *Astron. J.* **117,** 508–520 (1999).
29. Richer, H. B. *et al.* Isochrones and luminosity functions for old white dwarfs. *Astrophys. J.* (in the press).
30. Matthews, K. & Soifer, B. T. The near infrared camera on the W.M. Keck telescope. *Exp. Astron.* **3,** 77–84 (1994).

Acknowledgements

The UK Infrared Telescope is operated by the Joint Astronomy Centre on behalf of the UK Particle Physics and Astronomy Research Council. Some of the data presented here were obtained at the W. M. Keck Observatory, which is operated as a scientific partnership

among the California Institute of Technology, the University of California and NASA. The Observatory was made possible by the support of the W. M. Keck Foundation. S.T.H. and S.J.S. were supported by the PPARC; B.R.O. was supported by FUTDI and a Hubble postdoctoral research fellowship.

Correspondence and requests for materials should be addressed to S.T.H. (e-mail: sth@ast.cam.ac.uk).

Tunnelling between the edges of two lateral quantum Hall systems

W. Kang*†, H. L. Stormer†‡, L. N. Pfeiffer†, K. W. Baldwin† & K. W. West†

** James Franck Institute and Department of Physics, University of Chicago, Chicago, Illinois 60637, USA*
† Bell Laboratories, Lucent Technologies, Murray Hill, New Jersey 07974, USA
‡ Department of Physics and Department of Applied Physics, Columbia University, New York, New York 1002, USA

The edge of a two-dimensional electron system in a magnetic field consists of one-dimensional channels that arise from the confining electric field at the edge of the system[1–3]. The crossed electric and magnetic fields cause electrons to drift parallel to the sample boundary, creating a chiral current that travels along the edge in only one direction. In an ideal two-dimensional electron system in the quantum Hall regime, all the current flows along the edge[4–6]. Quantization of the Hall resistance arises from occupation of N one-dimensional edge channels, each contributing a conductance of e^2/h (refs 7–11). Here we report differential conductance measurements, in the integer quantum Hall regime, of tunnelling between the edges of a pair of two-dimensional electron systems that are separated by an atomically precise, high-quality, tunnel barrier. The resultant interaction between the edge states leads to the formation of new energy gaps and an intriguing dispersion relation for electrons travelling along the barrier: for example, we see a persistent conductance peak at zero bias voltage and an absence of tunnelling features due to electron spin. These features are unexpected and are not consistent with a model of weakly interacting edge states. Remnant disorder along the barrier and charge screening may each play a role, although detailed numerical studies will be required to elucidate these effects.

The one-dimensional edge channels of a two-dimensional electron system (2DES) in the quantum Hall regime represent a prototypical one-dimensional electronic system. Other such one-dimensional model systems include semiconductor-based quantum wires[12], carbon nanotubes[13,14], and molecular chain materials[15]. While these systems force the electrons to move along a preferential direction, the edge channels of a 2DES in the quantum Hall regime are unique in their ability to adjust themselves spatially as well as energetically. A localized defect is easily avoided by the edge current by simply skirting the impurity potential. In real samples, variations in the potential landscape can generate a complex topology of edge channels[16,17]. Consequently, most real edge channels are ill defined, both spatially and energetically, and it becomes difficult to generalize various experimental geometries in terms of one-dimensional edge states. Although typical experiments seek to study edge states in lithographically defined geometries[18,19], such edges typically fluctuate on the scale of a magnetic length. In order to address the energetics of edge channels, well-defined geometries with clearly delineated edges are essential. For tunnelling experiments in particular, where distance factors exponentially into the tunnelling current, exact knowledge of the shape and the magnitude of the barrier is crucial when comparing experimental results with model calculations.

Our 2DES–barrier–2DES (2D-2D) tunnelling device consists of two stripes of 2DES separated by an atomically precise 88-Å-thick semiconductor barrier, fabricated by cleaved edge overgrowth (Fig. 1a). We explore the lateral tunnelling between these two physically separated 2DESs in the quantum Hall regime, as shown in Fig. 1b. Figure 1c shows the differential conductance of the high-density sample at 9.2 T and 6.0 T. At 9.2 T, dI/dV_{bias} (where I is the current, and V_{bias} is bias voltage) is strongly suppressed around zero bias, while oscillatory conductance peaks appear above a threshold electric field. Each peak represents the onset of an additional tunnelling path through the barrier. Successive conductance peaks are nearly equally spaced, with a spacing of the order of the cyclotron energy $\hbar\omega_c$ (~17 meV at 10 T), and the amplitude of their oscillation decreases with increasing V_{bias}. Most of the traces of dI/dV_{bias} resemble the 9.2-T conductance data. But for certain ranges of magnetic field, B, there is no threshold to tunnelling, and a very sharp and intense conductance peak arises at zero bias, as illustrated by the 6-T data in Fig. 1c, lower panel.

Figure 2 shows an image map of the dI/dV_{bias} data as a function of Landau level filling factor, $\nu = nh/eB$ (where n is electron density and e is electron charge) and the normalized bias voltage, $eV_{bias}/\hbar\omega_c$. Blue and red represent small and large dI/dV_{bias} signals, respectively. With scaled axes, the disparate data from two different samples with

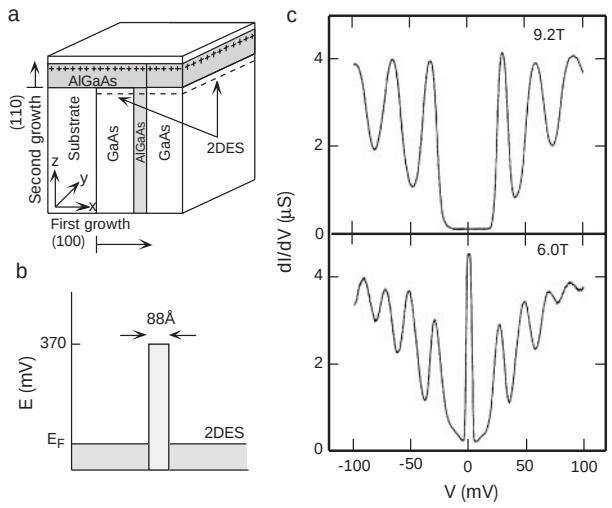

Figure 1 Structure and differential conductance measurements of our 2D-2D tunnelling device. **a**, The junctions are fabricated by cleaved edge overgrowth in molecular beam epitaxy (MBE)[22,23]. The first growth on a standard (100)GaAs substrate consists of an undoped 13-μm GaAs layer followed by an 88-Å-thick digital alloy of undoped $Al_{0.1}Ga_{0.9}As$/AlAs, and completed by a 14-μm layer of undoped GaAs. This triple-layer sample is cleaved along the (110) plane in an MBE machine and a modulation-doping sequence is grown over the exposed edge. It consists of a 3,500-Å-thick AlGaAs layer, delta-doped with Si at a distance of 500 Å from the interface. Carriers from the Si impurities transfer only into the GaAs layers of the cleaved edge, forming two stripes of 2DES of widths 13 μm and 14 μm, separated from each other by an 88-Å-thick, 370-meV-high $Al_{0.1}Ga_{0.9}As$/AlAs barrier. The sample is fabricated into a mesa incorporating the barrier and the two 2DESs. Contacts are made to the 2DESs, far away from the tunnelling region. **b,** Schematic band structure of the 2D-2D tunnelling device. Two different samples with electron density of $n = 1.1\times10^{11}cm^{-2}$ and $n = 2.0\times10^{11}cm^{-2}$ are studied. From a simultaneously grown monitor wafer, we estimate the mobility of the 2DESs in the device to be $\sim1\times10^5 cm^2\,V^{-1}\,s^{-1}$. **c,** Two representative traces of differential conductance through the tunnelling barrier with electron density $n = 2.0\times10^{11}cm^{-2}$. A low-frequency a.c. technique (typically 10 μV amplitude) is employed to measure the differential conductance, dI/dV_{bias}, through the barrier in the presence of a d.c. voltage bias, V_{bias}. The samples are measured at $T = 300$ mK in a magnitude field. Differential conductances, dI/dV_{bias}, nearly vanish near zero bias, while conductance oscillations of the order of $10^{-6}\,\Omega^{-1}$ are found at high bias.